이학석사학위논문

Resonance restoration of terahertz metamaterials in thinner film

두께의 얇아짐에 따른 테라헤르츠 메타물질의 공진주파수 복원

2017 년 2 월

서울대학교 대학원

물리천문학부

김 다 솜

Resonance restoration of terahertz metamaterials in thinner film

두께의 얇아짐에 따른 테라헤르츠 메타물질의 공진주파수 복원

지도교수 김 대 식

이 논문을 이학석사 학위논문으로 제출함

2017 년 2 월

서울대학교 대학원

물리천문학부

김 다 솜

김다솜의 석사학위논문을 인준함

2017 년 2 월

위 원 장 _____ (인)

부위원장 _____ (인)

위 원 _____ (인)

Abstract

High demands on metamaterials with desired resonance frequency and high field enhancement led to an extensive investigation on the sub-wavelength gaps, especially in terms of structural parameters. The role of most parameters including gap width, length, period and dielectric environment are widely studied and well understood, while the effect of metal thickness on the gap performance still remains elusive. Here, we theoretically and experimentally investigate resonance frequencies and field enhancements of sub-wavelength gaps with different heights. Scope of this study encompasses thicknesses as small as 10 nm, accessing by far the thinnest terahertz nano-resonators reported in the literature. The thickness decrease leads to huge field enhancement and resonance blueshift in transmission spectra of the sub-10nm gaps, restoring the transmission from the initially gap-plasmon dominated, red-shifted spectra. Such behavior is interpreted as a result of decreased effective refractive index of the gap, which is also supported by a modal-expansion analysis.

Keywords: terahertz transmission, terahertz time-domain spectroscopy, nanogap, ion-milling, Modal-expansion.

Student Number: 2015-20319

Contents

List of Figures

Chapter 1

Introduction

Terahertz metamaterials (THz MMs) for unusual electric and magnetic responses in THz regime have been developed over the past decade since the pioneering work by Yen et al [1]. For instance, spit ring resonators [1-3], negative refractive index metamaterials [4-6], high refractive index material [7], phase modulator [8], perfect absorber [9,10], and sub-wavelength gaps have been widely studied as THz MMS. Especially sub-wavelength THz gaps can incorporate high electric field enhancement (FE) due to high dielectric constant of surrounding metal and longer wavelength [11] which find uses in nonlinear optics [12,13], biological research [14,15], as well as pursuit of fundamentals of electromagnetism [16-20]. The initial studies regarding aforementioned purposes were conducted on gaps ranging in width from 100 um to 200 nm [16,19]. In this regime, the gap performance is dominated mainly by the gap width, length, and dielectric environment. Thickness of the gap has not attracted much attention since it barely affects the FE and induces very small redshift in transmission cutoff resonance frequency for thinner gaps [21-23]. Very recent researches on nanometer or angstrom wide gaps [19,20,24] indicate that completely new physics enters in the ultra-narrow gap width regime, calling for additional investigations on previously alienated variables. In this work, we report thickness dependent performance of sub-10 nm wide gaps and find out that thickness is a dominant factor in the gap

performance. We experimentally and theoretically demonstrate that FE as high as 7600 can be obtained at relatively high frequency of 1 THz, and the cutoff resonance is blue-shifted very sensitively as thickness contrary to properties reported previously. We understand the physical origin of this phenomenon from newly developed coupled mode method (CMM) [25,26] for both FE and cutoff resonance at sub-10 nm wide gaps.

Chapter 2

Fabrication of the nano-gap samples

In order to accurately control the gap widths of below 10 nm, we fabricate 2D periodic arrays of ring-shaped nano-gaps based on the atomic layer lithography [20]. Thickness of the gap is manipulated via glancing-angle ion milling [27] which was previously used for planarization of the sample. This method enables us to exclude effects from factors other than thickness of the sample and to make very thin samples. As shown schematically in Fig. 1(a), nano-gaps patterned under parameters l_1 and l_2 are fabricated into the 220 nm of Au film deposited onto Quartz. Top view of scanning electron microscope (SEM) images is shown in Fig. 1(b). Thickness of nano-gaps (h) is varied from 10 nm to 150 nm for several different gap widths (w). Fig. 1(c) are cross-sectional view of SEM images for h = 220 nm (top) after atomic layer lithography, and h = 90 nm (bottom) which is processed by glancing-angle ion milling at the top of h = 220 nm sample. While previous works [20,24] had difficulties in making the sub-30 nm thick nano-gaps due to island formation issues in physical deposition of thin films, glancing-angle ion milling is successfully leads to h = 10 nm sample as indicated in cross-sectional transmission electron microscope (TEM) image, Fig1. (d). It shows curved structure at the bottom of the gap since the contact angle between Quartz substrate and deposited Au cannot be atomically perpendicular.

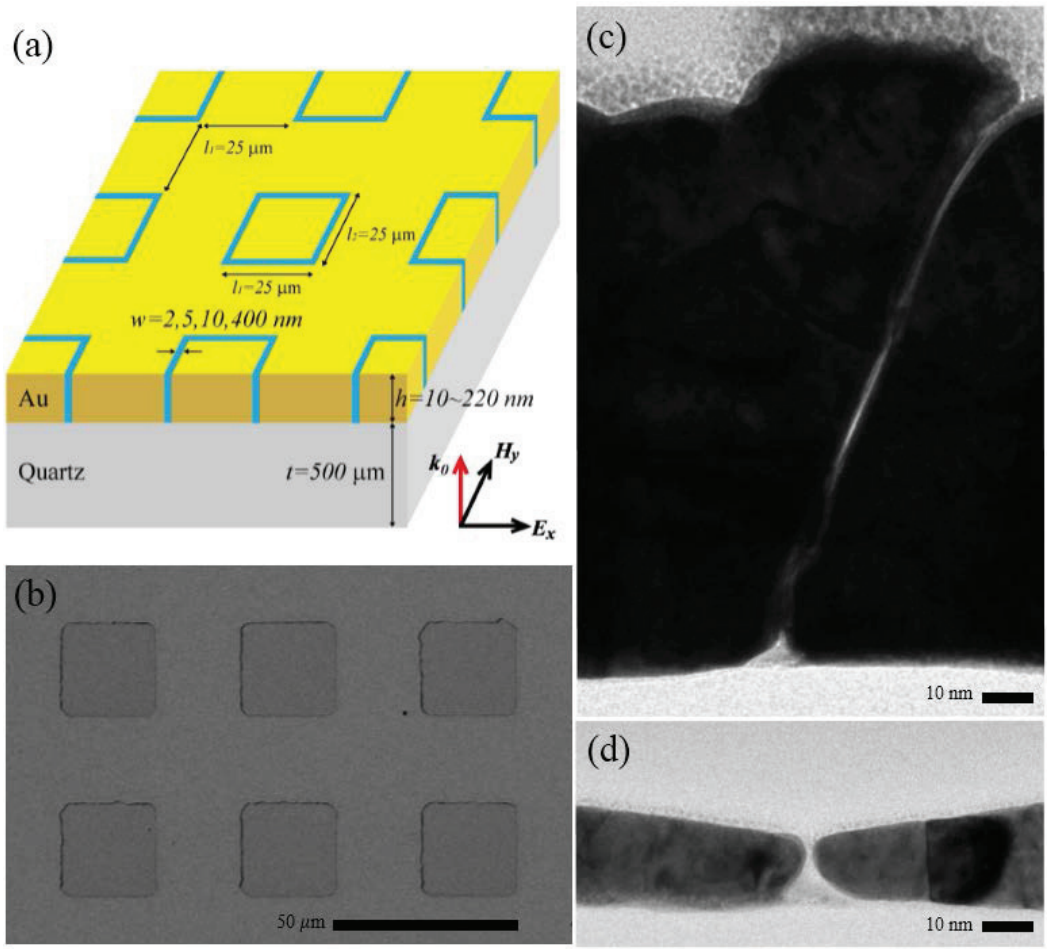

Figure 1: (a) Schematics of the sample; (b) An SEM image of the sample; (c) Cross sectional TEM image of the sample showing 2 nm gaps; (d) Ion-milled nano gap sample showing recovered aspect ratio.

Chapter 3

Terahertz time-domain spectroscopy of nano-gap samples

Next, we conduct far-field THz time-domain spectroscopy (TDS) over a frequency range of 0.2-1.4 THz on the gaps after each step of milling. Transmitted amplitudes are collected for the following samples: 2 nm gap (w = 2 nm, h = 10, 50, 90, 110, 130 nm, and 150 nm, see Fig. 2), 5 nm gap (w = 5 nm, h = 10, 30, 50, 70, 90, 110 nm, and 130 nm), 10 nm gap (w = 10 nm, h = 10, 30, 50, 70, 90, 110 nm, 130 nm), and 400 nm gap (w = 400 nm, h = 20 nm, 50 nm, see inset of Fig. 2). A p-polarized waves passes through 3mm * 3mm aluminum aperture and normally impinges on the samples. We measure the far-field transmissions of depicted samples and divided them with those of bare Quartz substrate to obtain normalized transmitted amplitudes. Near-field E_x enhancement is estimated from obtained amplitude by employing Kirchhoff integral formalism [29] after appropriately removing the effect from direct transmission through metal film. Fig. 2 presents frequency spectra of transmitted amplitudes and FEs of 2 nm gap for different thicknesses. As we decrease thickness from 150 nm to 10 nm, we discover two interesting features; (i) The FE increases by 6 folds (1300 to 7600) and (ii) the cutoff resonance dramatically is blue-shifted by 3 folds (0.33 to 1.10 THz). This observation directly contrasts the previous reports where thickness change is more or less irrelevant to FE or cutoff resonance of the gap. Moreover, the FE of 7600 is the strongest ever

reported at frequencies above 1 THz in elongated gaps, considering that FE in high frequency is normally lower than that of lower frequency [11,17]. On the other hand, the inset of Fig. 2 shows contrary behavior where cutoff resonance of 400 nm gap is slightly red-shifted from 1.33 to 1.28 THz, due to dielectric substrate effect as theoretically reported previously [21,22]. More detailed physical origin of the thickness dependences and the contrary behaviors between 2 nm gap and 400 nm gap will later be given.

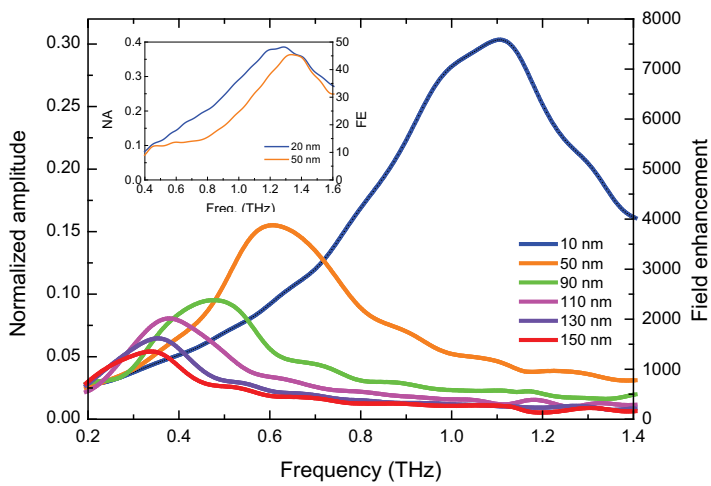

Figure 2: Transmission spectrum of 2 nm gap sample with different thickness. The inset is of 400 nm gap sample.

Chapter 4

Coupled mode method

In pursuance of the physical origin of the results presented above, we perform the theoretical calculation using coupled-mode method established on the modal expansion of the electromagnetic fields. Garcia-Vidal et al [25,30] provides the fundamental of the formalism. Although the thickness of the metal is thinner than skin-depth (~170 nm for 0.2 THz), direct transmission through the metal film of 10 nm is experimentally less than 3 % due to the huge reflection on the front metal surface allowing us to apply this formalism to our works [31]. Also, the effect of gap plasmon, coupling between surface plasmon polaritons on two side-walls of the gap, is expected to come into play since, ($\frac{w}{\lambda} \sim \frac{\epsilon_d}{\epsilon_m}$), in the regime of our interest [32], where ϵ_m is the dielectric parameters of the metal [33] and ϵ_d is dielectric constant of material (Aluminum) inside the gaps [34,35]. Therefore, our calculation combines the formalism of an array of rectangular gap in real a metal [25,36,37] and of effective index mode [38] which contains gap plasmon effect in rectangular waveguide in terahertz regime. By matching the EM fields at the interfaces, we obtain modal amplitudes of the electric field at the input and output sides of the gap, E and E', via a set of two coupled linear equations:

$$\left(G^{I} - \Sigma\right)\mathrm{E} - G_V E' = I_0,$$

$$\left(G^{III} - \Sigma\right)E' - G_V\mathrm{E} = 0.$$

The term I_0 represents the external illumination on the gap for normal incidence:

$$I_0 = \frac{i\sqrt{2}}{1+Z_s}\frac{\frac{2l}{\pi}\sin(\frac{\pi l_2}{2l})}{\frac{l}{2\pi}\sin(\frac{\pi l_2}{l})+\frac{l_2}{2}},$$

where $Z_s = \frac{1}{\sqrt{\epsilon_m(\omega)}}$ is surface impedance of the metal and l is half length of the rectangular ring, $l = l_1 + l_2$. The terms Σ and G_V are applied as presented in [36], while the admittance Y_{TE} and propagation constant of fundamental TE mode inside the rings q_z are replaced with following expressions to consider leaking wave vector into the metal:

$$Y_{TE} = \frac{q_z}{k_0(1+\frac{k_1^2}{\epsilon_d k_0^2})},\ q_z = \sqrt{\epsilon_d k_0^2 + k_1^2 - (\frac{\pi}{l})^2}$$

where, k_1 is the magnitude of leaking wave vector into the metal (gap plasmon) whose amplitude is given by[38]:

$$k_1^2 = -\frac{1+\sqrt{1-4k_o^2(\epsilon_m-\epsilon_d)\left(\frac{w\epsilon_m}{2\epsilon_d}\right)^2}}{\left(\frac{\epsilon_m}{\epsilon_d}\right)^2}.$$

EM coupling between the gaps is controlled by the term G^{I} and G^{III},

$$G^{\mathrm{I,III}} = \sum_{mn}\frac{iw}{l_1}\frac{\epsilon_{\mathrm{I,III}}k_o^2 - k_{y\_n}^2}{(k_0+Z_s k_{\mathrm{I,III}z})k_{\mathrm{I,III}z}}\left|\mathrm{sinc}\left(\frac{wk_{x\_m}}{2}\right)[\mathrm{sinc}\left(\frac{\pi}{2}+\frac{lk_{y_n}}{2}\right)+\mathrm{sinc}\left(\frac{\pi}{2}-\frac{lk_{y_n}}{2}\right)]\right|^2, (1)$$

with $k_{\mathrm{I,III}z} = \sqrt{\epsilon_{\mathrm{I,III}}k_o^2 - k_{x\_m}^2 - k_{y\_n}^2}$, $k_{x\_m} = \frac{2\pi m}{d_x}$, $k_{y\_n} = \frac{2\pi n}{d_y}$, $k_0 = \frac{2\pi}{\lambda}$ (m and n are integer, $\epsilon_{\mathrm{I,III}}$ are dielectric constant of the substrate and air, respectively).

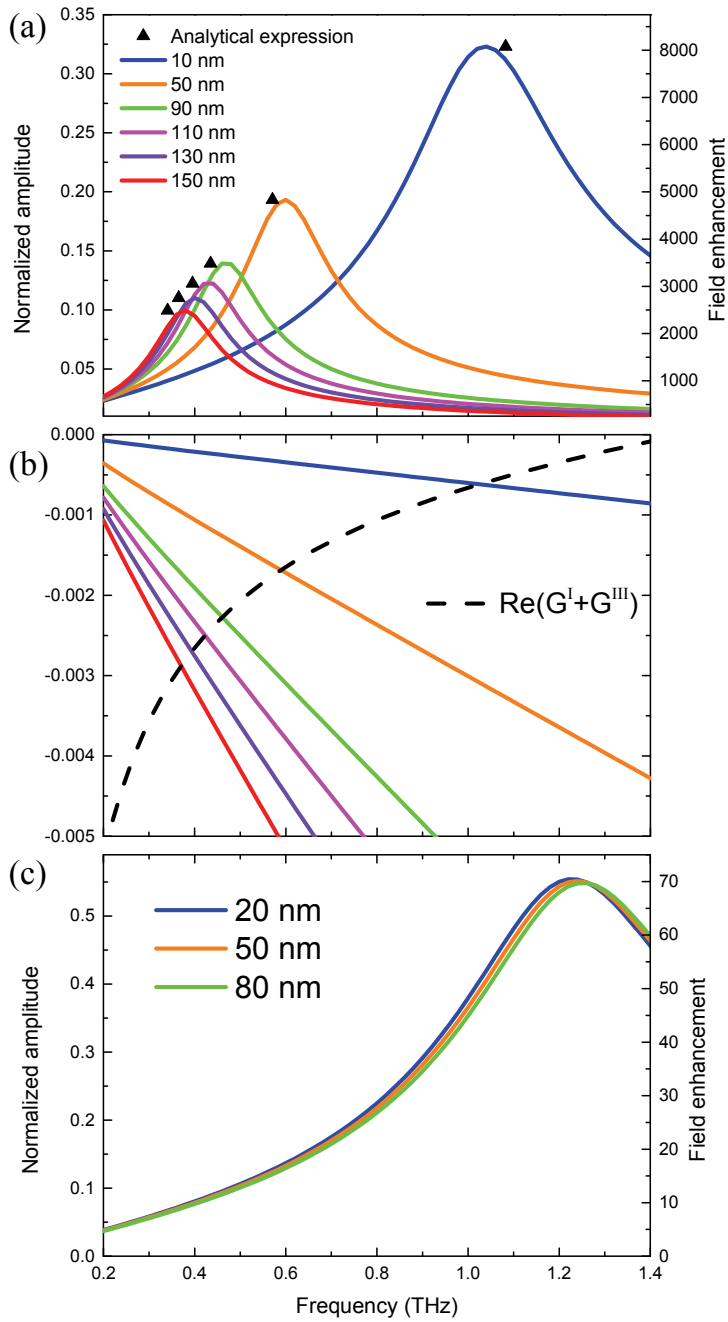

Figure 3: (a) Calculated transmission spectrum of 2 nm gap sample with different thickness. (b) For the same system as that in the (a) panel, the dashed line depicts $Re(G^{I} + G^{III})$ as a function of frequency. Straight lines correspond to the right-hand side of Eq. (2). (c) Calculated transmission spectrum of 400 nm gap sample with different thickness.

Fig. 3 depicts our numerical calculation presented above, which clearly shows increased FE in thinner film. In case of 2 nm gap (a), remarkable blue-shifted spectra appear in thinner film, while in case of 400 nm gap (c), slightly red-shifted spectrum is presented. Well quantitative agreement between the theoretical calculation and the regarding experimental results shown in Fig. 2(a) (even without any fitting parameter).

Now, we qualitatively concentrate on physics underlying the two different phenomena. First, for very *thin* films ($h \sim 0$ nm) the cutoff resonance of both 2 nm gap and 400 nm gap is only controlled by the coupling of the gap to radiative regions, $G \sim 0$ (substrate effect). As a result, they have almost same cutoff resonance, $f_{res} \approx \frac{c_0}{2l\sqrt{\epsilon_a}}$ where $\epsilon_a = \frac{\epsilon_{I} + \epsilon_{III}}{2}$, c_0 is the speed of the light in vacuum [21,39]. On the other hand, when it comes to relatively *thick* film regime, the cutoff resonance tends to follows properties of waveguide slightly losing the substrate effect (blueshift). Considering that the ratio of gap plasmon effect to propagation constant is $\frac{Re(k_1^2)}{Re(q_z^2)} \sim 0.05$ for $w = 400$ nm and $\frac{Re(k_1^2)}{Re(q_z^2)} \sim 1$ for $w = 2$ nm at near the cutoff resonance, we recognize 400 nm gap is only controlled by the properties of the waveguide possessing *a higher* cutoff resonance, while in case of the 2 nm gap, the cutoff resonance is controlled by properties of waveguide possessing *a lower* cut-off frequency since gap plasmon strongly makes the cutoff resonance red-shifted [38].

Now, we attempt to understand the phenomena quantitatively by explicitly expressing the resonance condition under various geometries. In our case, electric

field at the output side is expressed as $E' = \frac{G_V I_0/\Sigma}{\{(G^{I}-\Sigma)(G^{III}-\Sigma)-G_V^2\}/\Sigma}$. We find that critical point occurs when its real part of the denominator is 0:

$$\mathrm{Re}\left(G^{I} + G^{III}\right) = Re(\Sigma - \frac{G_V^2}{\Sigma}), \quad (2)$$

where second-order term of G^{I}, G^{III} is approximated to zero for sub-wavelength gap limit. Fig. 3(b) shows the graphical solution of equation (2) in case of 2 nm gap. It renders the dependence of both $Re\left(G^{I} + G^{III}\right)$ and $Re(\Sigma - \frac{G_V^2}{\Sigma})$ versus frequency for several values of h = 10, 50, 90, 110, 130 nm, 150 nm (note that $Re\left(G^{I} + G^{III}\right)$ does not change on h, see Eq. (1)). As indicated by dotted lines in Fig. 3(a) and (b), cutoff resonance appears when two values of the expression are the same. For further understanding of this phenomenon, getting the analytical expression is helpful. For our case where the gap plasmon effect is dominant, assuming $h \ll \lambda$, $\sqrt{\epsilon_m} \sim 500(1+i)$, leading to the following spectral characteristic equation:

$$f_{res} \approx \frac{c_0/2l}{\sqrt{\epsilon_a + \frac{\epsilon_d h}{3w}}}.$$

From the expression, one can realize the term $\frac{\epsilon_d h}{3w}$ reflects the newly introduced gap plasmon effect. Also, we notice that a gap can be considered as substrate-free when $\epsilon_d h \gg w$. From the aforementioned resonance condition, we also analyze the resonance FE of the gap, which can be obtained from the expression of E' under the resonance condition. After several steps of simple algebra and approximation, we find:

$$E'_{res} \approx \frac{I_0}{Im\left(G^{I}+G^{III}\right)+Re\left(\sqrt{\epsilon_m}\right)\frac{wh}{2}\left(\frac{\pi}{l}\right)^2}, with\ f = f_{res}. \quad (3)$$

The above analytical expressions for cutoff resonance frequency and FE is plotted as triangles in Fig. 3(a). The expressions follow the full calculation results very well, with error being slightly longer for extremely thin sample. Also, the term $Re(\sqrt{\epsilon_m})\frac{wh}{2}(\frac{\pi}{l})^2$ in Eq. (3) reflects the gap plasmon effect. These relations imply that the cutoff resonance transmission is a complex function of film thickness, gap width, length, and dielectric environment. Also, considering that $Im\left(G^{I}+G^{III}\right)$ is almost constant under change of h, we expect thickness-dependent resonance FE in a form of $\frac{1}{\alpha+\beta h}$ where α, β are constant. Fig. 4 represents the FE with different gap width (dots), well following a $\frac{1}{\alpha+\beta h}$-type thickness dependence denoted as black lines. We perceive that there is an ultimate value when the thickness is nearly zero.

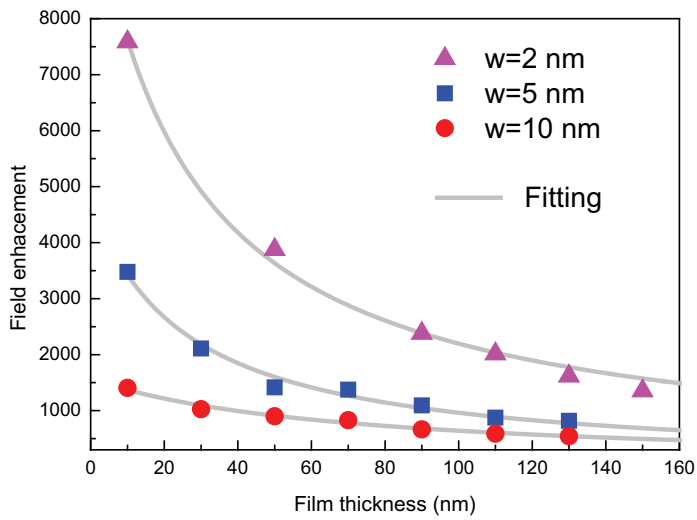

Figure 4: Measured field enhancement at resonance frequency as a function of film thickness (dot). The fits (gray line) indicate $\frac{1}{\alpha+\beta h}$-type thickness dependence.

Chapter 5

Conclusion

In conclusion, we fabricate very thin-film THz MMS and experimentally demonstrate unusual electromagnetic response where the cutoff resonance is blue-shifted and electric FE increases dramatically with decreasing thickness. Theoretical analysis based on the modal expansion is also given demonstrating that the origin of the response mainly comes from the gap plasmon effect. We derive analytical expression for the performance of sub-10 nm wide gaps which are of great interest in nano- or angstrom optics. Our results open up intriguing possibility of substrate free nonlinear optics and sensing devices with extremely high FE previously unreachable.

References

1. Yen, T. J.; Padilla, W. J.; Fang, N.; Vier, D. C.; Smith, D. R.; Pendry, J. B.; Basov, D. N.; Zhang, X., Terahertz magnetic response from artificial materials. Science 2004, 303 (5663), 1494-1496.
2. Chen, H. T.; Padilla, W. J.; Zide, J. M. O.; Gossard, A. C.; Taylor, A. J.; Averitt, R. D., Active terahertz metamaterial devices. Nature 2006, 444 (7119), 597-600.
3. Padilla, W. J.; Aronsson, M. T.; Highstrete, C.; Lee, M.; Taylor, A. J.; Averitt, R. D., Electrically resonant terahertz metamaterials: Theoretical and experimental investigations. Phys Rev B 2007, 75 (4).
4. Yannopapas, V.; Moroz, A., Negative refractive index metamaterials from inherently non-magnetic materials for deep infrared to terahertz frequency ranges. J Phys-Condens Mat 2005, 17 (25), 3717-3734.
5. Paul, O.; Imhof, C.; Reinhard, B.; Zengerle, R.; Beigang, R., Negative index bulk metamaterial at terahertz frequencies. Opt Express 2008, 16 (9), 6736-6744.
6. Weis, P.; Paul, O.; Imhof, C.; Beigang, R.; Rahm, M., Strongly birefringent metamaterials as negative index terahertz wave plates. Appl Phys Lett 2009, 95 (17).
7. Choi, M.; Lee, S. H.; Kim, Y.; Kang, S. B.; Shin, J.; Kwak, M. H.; Kang, K. Y.; Lee, Y. H.; Park, N.; Min, B., A terahertz metamaterial with unnaturally high refractive index. Nature 2011, 470 (7334), 369-373.
8. Chen, H. T.; Padilla, W. J.; Cich, M. J.; Azad, A. K.; Averitt, R. D.; Taylor, A. J., A metamaterial solid-state terahertz phase modulator. Nat Photonics 2009, 3

(3), 148-151.

9. Tao, H.; Landy, N. I.; Bingham, C. M.; Zhang, X.; Averitt, R. D.; Padilla, W. J., A metamaterial absorber for the terahertz regime: Design, fabrication and characterization. Opt Express 2008, 16 (10), 7181-7188.
10. Landy, N. I.; Sajuyigbe, S.; Mock, J. J.; Smith, D. R.; Padilla, W. J., Perfect metamaterial absorber. Phys Rev Lett 2008, 100 (20).
11. Kang, J. H.; Kim, D. S.; Park, Q. H., Local Capacitor Model for Plasmonic Electric Field Enhancement. Phys Rev Lett 2009, 102 (9).
12. Kim, J. Y.; Kang, B. J.; Park, J.; Bahk, Y. M.; Kim, W. T.; Rhie, J.; Jeon, H.; Rotermund, F.; Kim, D. S., Terahertz Quantum Plasmonics of Nanoslot Antennas in Nonlinear Regime. Nano Lett 2015, 15 (10), 6683-6688.
13. Bahk, Y. M.; Kang, B. J.; Kim, Y. S.; Kim, J. Y.; Kim, W. T.; Kim, T. Y.; Kang, T.; Rhie, J.; Han, S.; Park, C. H.; Rotermund, F.; Kim, D. S., Electromagnetic Saturation of Angstrom-Sized Quantum Barriers at Terahertz Frequencies. Phys Rev Lett 2015, 115 (12).
14. Park, H. R.; Ahn, K. J.; Han, S.; Bahk, Y. M.; Park, N.; Kim, D. S., Colossal Absorption of Molecules Inside Single Terahertz Nanoantennas. Nano Lett 2013, 13 (4), 1782-1786.
15. Lee, D. K.; Kang, J. H.; Lee, J. S.; Kim, H. S.; Kim, C.; Kim, J. H.; Lee, T.; Son, J. H.; Park, Q. H.; Seo, M., Highly sensitive and selective sugar detection by terahertz nano-antennas. Sci Rep-Uk 2015, 5.
16. Lee, J. W.; Seo, M. A.; Kang, D. H.; Khim, K. S.; Jeoung, S. C.; Kim, D. S., Terahertz electromagnetic wave transmission through random arrays of single

rectangular holes and slits in thin metallic sheets. Phys Rev Lett 2007, 99 (13).

17. Seo, M. A.; Park, H. R.; Koo, S. M.; Park, D. J.; Kang, J. H.; Suwal, O. K.; Choi, S. S.; Planken, P. C. M.; Park, G. S.; Park, N. K.; Park, Q. H.; Kim, D. S., Terahertz field enhancement by a metallic nano slit operating beyond the skin-depth limit. Nat Photonics 2009, 3 (3), 152-156.
18. Park, H. R.; Bahk, Y. M.; Ahn, K. J.; Park, Q. H.; Kim, D. S.; Martin-Moreno, L.; Garcia-Vidal, F. J.; Bravo-Abad, J., Controlling Terahertz Radiation with Nanoscale Metal Barriers Embedded in Nano Slot Antennas. Acs Nano 2011, 5 (10), 8340-8345.
19. Bahk, Y. M.; Park, H. R.; Ahn, K. J.; Kim, H. S.; Ahn, Y. H.; Kim, D. S.; Bravo-Abad, J.; Martin-Moreno, L.; Garcia-Vidal, F. J., Anomalous Band Formation in Arrays of Terahertz Nanoresonators. Phys Rev Lett 2011, 106 (1).
20. Chen, X. S.; Park, H. R.; Pelton, M.; Piao, X. J.; Lindquist, N. C.; Im, H.; Kim, Y. J.; Ahn, J. S.; Ahn, K. J.; Park, N.; Kim, D. S.; Oh, S. H., Atomic layer lithography of wafer-scale nanogap arrays for extreme confinement of electromagnetic waves. Nat Commun 2013, 4.
21. Carretero-Palacios, S.; Garcia-Vidal, F. J.; Martin-Moreno, L.; Rodrigo, S. G., Effect of film thickness and dielectric environment on optical transmission through subwavelength holes. Phys Rev B 2012, 85 (3).
22. Kang, J. H.; Choe, J. H.; Kim, D. S.; Park, Q. H., Substrate effect on aperture resonances in a thin metal film. Opt Express 2009, 17 (18), 15652-15658.
23. Shou, X.; Agrawal, A.; Nahata, A., Role of metal film thickness on the enhanced transmission properties of a periodic array of subwavelength apertures. Opt

Express 2005, 13 (24), 9834-9840.

24. Jeong, J.; Rhie, J.; Jeon, W.; Hwang, C. S.; Kim, D. S., High-throughput fabrication of infinitely long 10 nm slit arrays for terahertz applications. J Infrared Millim Te 2015, 36 (3), 262-268.
25. Garcia-Vidal, F. J.; Martin-Moreno, L.; Ebbesen, T. W.; Kuipers, L., Light passing through subwavelength apertures. Rev Mod Phys 2010, 82 (1), 729-787.
26. Bravo-Abad, J.; Garcia-Vidal, F. J.; Martin-Moreno, L., Resonant transmission of light through finite chains of subwavelength holes in a metallic film. Phys Rev Lett 2004, 93 (22).
27. Yoo, D.; Nguyen, N. C.; Martin-Moreno, L.; Mohr, D. A.; Carretero-Palacios, S.; Shaver, J.; Peraire, J.; Ebbesen, T. W.; Oh, S. H., High-Throughput Fabrication of Resonant Metamaterials with Ultrasmall Coaxial Apertures via Atomic Layer Lithography. Nano Lett 2016, 16 (3), 2040-2046.
28. Han, S.; Bahk, Y. M.; Park, N.; Kim, D. S., Terahertz field enhancement in asymmetric and tapered nano-gaps. Opt Express 2016, 24 (3), 2065-2071.
29. Kyoung, J. S.; Seo, M. A.; Park, H. R.; Ahn, K. J.; Kim, D. S., Far field detection of terahertz near field enhancement of sub-wavelength slits using Kirchhoff integral formalism. Opt Commun 2010, 283 (24), 4907-4910.
30. Garcia-Vidal, F. J.; Moreno, E.; Porto, J. A.; Martin-Moreno, L., Transmission of light through a single rectangular hole. Phys Rev Lett 2005, 95 (10).
31. de Leon-Perez, F.; Brucoli, G.; Garcia-Vidal, F. J.; Martin-Moreno, L., Theory on the scattering of light and surface plasmon polaritons by arrays of holes and dimples in a metal film. New J Phys 2008, 10.

32. Bozhevolnyi, S. I.; Jung, J., Scaling for gap plasmon based waveguides. Opt Express 2008, 16 (4), 2676-2684.
33. Ordal, M. A.; Long, L. L.; Bell, R. J.; Bell, S. E.; Bell, R. R.; Alexander, R. W.; Ward, C. A., Optical-Properties of the Metals Al, Co, Cu, Au, Fe, Pb, Ni, Pd, Pt, Ag, Ti, and W in the Infrared and Far Infrared. Appl Optics 1983, 22 (7), 1099-1119.
34. Groner, M. D.; Elam, J. W.; Fabreguette, F. H.; George, S. M., Electrical characterization of thin Al2O3 films grown by atomic layer deposition on silicon and various metal substrates. Thin Solid Films 2002, 413 (1-2), 186-197.
35. Bareiss, M.; Hochmeister, A.; Jegert, G.; Zschieschang, U.; Klauk, H.; Huber, R.; Grundler, D.; Porod, W.; Fabel, B.; Scarpa, G.; Lugli, P., Printed array of thin-dielectric metal-oxide-metal (MOM) tunneling diodes. J Appl Phys 2011, 110 (4).
36. Mary, A.; Rodrigo, S. G.; Martin-Moreno, L.; Garcia-Vidal, F. J., Theory of light transmission through an array of rectangular holes. Phys Rev B 2007, 76 (19).
37. Garcia-Vidal, F. J.; Martin-Moreno, L.; Moreno, E.; Kumar, L. K. S.; Gordon, R., Transmission of light through a single rectangular hole in a real metal. Phys Rev B 2006, 74 (15).
38. Gordon, R.; Brolo, A. G., Increased cut-off wavelength for a subwavelength hole in a real metal. Opt Express 2005, 13 (6), 1933-1938.
39. Choe, J. H.; Kang, J. H.; Kim, D. S.; Park, Q. H., Slot antenna as a bound charge oscillator. Opt Express 2012, 20 (6), 6521-6526.

국문초록

원하는 공진 주파수 및 높은 장 집속능력을 갖는 나노 공진기는 고주파 생성, 분자 감지 및 비선형 광학 등, 많은 분야에서 사용된다. 이를 위해, 갭 폭, 길이 및 주기를 포함하는 나노 공진기의 다양한 구조상수가 최적화되었지만, 금속 두께가 공진기의 성능에 미치는 영향은 아직 미지의 영역으로 남아있다. 이 연구에서는 서로 다른 금속 두께를 갖는 나노 공진기에서 공진 주파수와 장 집속능력을 조사한다. 이 연구는 10 ㎚ 정도로 얇은 두께를 가진 나노 공진기를 제작하는 방법을 소개하고 그 특성을 연구한다. 공진기의 두께가 얇아지면 갭 플라즈몬효과에 의해 적색편이 되었던 공진주파수의 회복과 함께 매우 높은 장 집속능력을 관찰 할 수 있다.